Research article
doi.org/10.1002/elsa.202100094

Chemistry Europe
European Chemical Societies Publishing

Received: 21 May 2021
Revised: 1 July 2021
Accepted: 12 July 2021

Potential dependent spectroelectrochemistry of electrofluorogenic dyes on indium-tin oxide

Vignesh Sundaresan[1,#] | **Allison R. Cutri**[2,#] | **Jarek Metro**[2] | **Chinedu S. Madukoma**[3,4] | **Joshua D. Shrout**[3,4,5] | **Anthony J. Hoffman**[6] | **Katherine A. Willets**[7] | **Paul W. Bohn**[1,2]

[1] Department of Chemical and Biomolecular Engineering, University of Notre Dame, Notre Dame, Indiana

[2] Department of Chemistry and Biochemistry, University of Notre Dame, Notre Dame, Indiana

[3] Department of Civil and Environmental Engineering and Earth Sciences, University of Notre Dame, Notre Dame, Indiana

[4] Eck Institute for Global Health, University of Notre Dame, Notre Dame, Indiana

[5] Department of Biological Sciences, University of Notre Dame, Notre Dame, Indiana

[6] Department of Electrical Engineering, University of Notre Dame, Notre Dame, Indiana

[7] Department of Chemistry, Temple University, Philadelphia, Philadelphia

Correspondence
Katherine A. Willets, Department of Chemistry, Temple University, Philadelphia, PA 19122.
Email: kwillets@temple.edu
Paul W. Bohn, Department of Chemical and Biomolecular Engineering, University of Notre Dame, Notre Dame, IN 46556.
Email: pbohn@nd.edu

[#]Vignesh Sundaresan and Allison R. Cutri contributed equally to the execution and analysis of these experiments.

Funding information
Department of Energy Office of Science, Grant/Award Number: DE-SC0019312; National Institute of Health, Grant/Award Number: R01 AI113219-06

Abstract

Indium-tin oxide (ITO) is used in a variety of applications due to its electrical conductivity and optical transparency. Moreover, ITO-coated glass is a common working electrode for spectroelectrochemistry. Thus, the ITO substrates should exhibit well-understood spectroscopic characteristics. Here, we report anomalous potential-dependent luminescence emission from three structurally dissimilar electrofluorogenic probe on ITO-coated glass. The three probes, flavin mononucleotide, resorufin, and Nile blue, show the expected fluorescence modulation between their oxidized, emissive forms and their reduced, nonfluorescent forms at low laser irradiance and/or high concentrations. However, at high irradiance and/or low concentration, the emission intensity increases at reducing potentials, contrary to expectations. In addition, a strong interplay between probe molecule concentration and laser irradiance is observed. We attribute the anomalous behavior to a combination of (1) irradiance-dependent ITO carrier dynamics, and (2) interaction of the fluorescent probe with ITO at reducing potentials resulting in a charge transfer state with altered emission behavior. Thus, the potential- and irradiance-dependent behavior of ITO and the resulting charge transfer state may not only interfere with the observation of potential-dependent fluorescence from redox probes but can completely reverse the polarity of the potential-dependent luminescence, especially at high irradiance and low concentration.

Research article
doi.org/10.1002/elsa.202100094
Chemistry Europe
European Chemical Societies Publishing

KEYWORDS
electrofluorogenic probes, flavin mononucleotide, fluorescence imaging, Indium-tin-oxide, spectroelectrochemistry

1 | INTRODUCTION

Spectroelectrochemical studies are valuable because they can provide rich mechanistic information about processes and phenomena occurring at the electrode–electrolyte interface, which cannot be obtained from traditional electrochemical measurements.[1] Spectroelectrochemistry has been employed to understand atomic/molecular mechanisms in electron transfer in a variety of technically relevant areas including bioelectrochemistry, energy conversion, and energy storage.[2] Advances in optical microscopy and spectroscopy, such as super-resolution imaging and surface-enhanced Raman scattering, have enabled spectroelectrochemical experiments at the nanoscale and with single entities (e.g. single particles or molecules).[3] For example, Zhang and coworkers have observed single redox events on porous silica-coated indium-tin oxide (ITO) electrodes using single-molecule fluorescence microscopy, in which a single electrofluorogenic redox probe (resorufin) modulates its fluorescence between high and low emission intensity based on the applied potential.[4] Chen and coworkers have used a similar system to study photoelectrochemical water splitting at TiO_2 nanorods dispersed on ITO with spatial and temporal resolutions of ~30 nm and ~15 ms, respectively.[5] In addition, a number of groups have studied the electrochemical behavior of individual nanoparticles.[6] For instance, Willets and coworkers used dark-field microscopy to observe the electrodissolution of single Ag nanoparticles,[7] using the correlation of scattering intensity and nanoparticle size to track electrodissolution in real time.

Spectroelectrochemistry can also be applied to microbial systems.[8] The spectroelectrochemistry of bacterial systems is significant, because it can provide a detailed understanding of the electron transfer process, potential-dependent conformation, and redox state of the enzymes within the microbe, and it also enables ultrasensitive detection of metabolites secreted by the microbes.[9] For example, Lynk et al. combined electrochemical and surface-enhanced Raman scattering to detect both Gram-positive and Gram-negative bacteria based on their nucleotide breakdown products.[10]

Many spectroelectrochemical experiments performed at the nanoscale and with single entities use ITO as the working electrode.[4,5,6b,11] ITO is an optically transparent conductive oxide widely used due to its unusual combination of conductivity and transparency. ITO is an n-type semiconductor in which the combination of large bandgap, $E_g \sim 4$ eV, and low electrical resistivity, $\rho \sim 10^{-4}$ Ω cm, are accompanied by high transmission throughout much of the visible and near-IR regions,[12] making it a nearly ideal substrate for spectroelectrochemical studies, such as fluorescence, electrogenerated chemiluminescence, and Raman scattering, at both bulk- and single-molecule levels.[13] Additionally, ITO can be coated on glass using vapor deposition, solution processing, and sputtering methods and is available commercially, making it a desirable and easily accessible material for use as an electrochemical substrate, as well as in solar cell panels, thin-film photovoltaics, and other smart technologies.[14]

Given the wide range of scientific and technological uses of ITO, it is important to understand its luminescence behavior in spectroelectrochemical experiments. Here, we use wide-field fluorescence imaging to show that the fluorescence response of electrofluorogenic redox probes near an ITO electrode changes as a function of applied potential and excitation laser irradiance. In one class of electrofluorogenic redox probes, the molecules are fluorescent in the oxidized state, but are much less fluorescent in the reduced state, so their fluorescence can be modulated between high and low emission states by applying suitable electrochemical potentials.[15] Surprisingly, under certain conditions with ITO electrodes, we observe just the opposite. This inverted response is observed with three different redox probes: flavin mononucleotide (FMN), Nile Blue (NB), and resorufin, which are excited at different wavelengths, suggesting that ITO plays an important role in the anomalous response. A systematic analysis shows that the potential-dependent fluorescence response, whether canonical or anomalous, is determined by an interplay between laser irradiance and the electrofluorogenic redox probe concentration. We attribute this behavior to a combination of irradiance-dependent ITO carrier dynamics, and interaction of the fluorescent probes with ITO at reducing potentials resulting in a charge transfer state with altered emission behavior. The work presented here shows that the background contribution from the ITO not only interferes with observation of the potential-dependent fluorescence behavior of the redox probes but is capable of completely reversing the polarity of the potential-dependence, especially at high irradiance and low concentration.

Research article
doi.org/10.1002/elsa.202100094
Chemistry Europe
European Chemical Societies Publishing

2 | MATERIALS AND METHODS

2.1 | Chemicals and materials

FMN, resorufin sodium salt, NB, potassium nitrate (KNO_3), sodium phosphate dibasic heptahydrate, sodium phosphate monobasic monohydrate, and phosphate buffer saline solution (PBS, pH 7.4) were purchased from Sigma–Aldrich. Indium-tin-oxide coated glass coverslips (ITO, #1 thickness, 22 × 22 mm, 15-30 Ω/sq resistivity) were purchased from SPI Supplies. A two-part silicone elastomer, polydimethylsiloxane (PDMS) was acquired from Polymer Sources, Inc. Silver conductive epoxy was obtained from Electron Microscopy Sciences. All chemicals were used as-received without further purification. Aqueous solutions were prepared using deionized (DI) water ($\rho = 18.2$ MΩ) from a Millipore Milli-Q system.

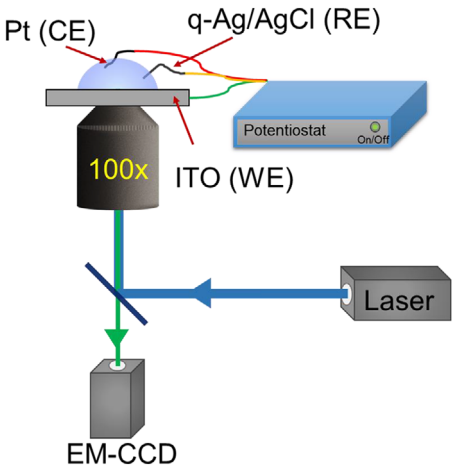

FIGURE 1 Schematic diagram showing the wide-field fluorescence apparatus used for spectroelectrochemical measurements

2.2 | Bacterial growth medium

Myxococcus xanthus (*M. xanthus*) wildtype DK1622 was used in this study.[16] Cells were streaked from frozen (−80°C) and maintained on CTT medium (1% Casitone, 10 mM Tris-HCl [pH 8.0], 8 mM $MgSO_4$, 10 mM KH_2PO_4 [pH 7.6]) solidified with 1.5% agar.[17] Liquid cultures were grown at 32°C in CTT broth with vigorous shaking. Cells at log-phase (optical density at 600 nm [OD_{600}] ≈ 2) were harvested and washed three times and resuspended in PBS prior to analysis.

2.3 | Sample preparation

ITO coverslips were cleaned in acetone, isopropyl alcohol, and DI water in an ultrasonicator for 15 min each and then dried with N_2. A copper wire was attached to the coverslip using a silver conductive epoxy to provide electrical contact, and a 5-6 mm diameter PDMS well was attached to the ITO surface using Devcon 5-min epoxy. FMN, resorufin, and NB solutions were prepared in aqueous 0.2 M KNO_3, which serves as the supporting electrolyte.

2.4 | Spectroelectrochemistry

The ITO-based spectroelectrochemical cell was mounted on an Olympus IX-71 inverted microscope equipped with a 100× objective (Olympus immersion, NA = 1.45). A schematic diagram of the spectroelectrochemical apparatus is shown in Figure 1. A 100 µL aliquot of the redox probe solution was then added to the PDMS well, and Pt and Ag/AgCl wires were placed in the well to serve as the counter and quasi-reference electrodes, respectively. All electrodes were then connected to a CH750E potentiostat (CH Instruments). Laser excitation was provided at 458, 532, and 643 nm for FMN, resorufin, and NB, respectively, and emission was collected through the objective and passed through a dichroic filter before being imaged onto a Peltier-cooled EMCCD camera (Andor iXon EMCCD for FMN, Princeton instruments PhotonMax 512 EMCCD for resorufin, and ProEM 512 for NB studies). Movies were recorded using an integration time of 0.1 or 0.05 s.

3 | RESULTS AND DISCUSSION

3.1 | Potential-dependent fluorescence of *Myxococcus xanthus*

Our initial goal was to understand the redox properties of *M. xanthus*, a soil-dwelling Gram-negative bacterium, by using flavin-derivatives as molecular sentinels. Flavoproteins are common electron carriers important to metabolism in bacteria and other organisms that utilize flavin-based electron carrier molecules, FMN and/or flavin adenine dinucleotide, with population estimates suggesting approximately 3×10^4 flavins expressed in mature cells, many in the outer membrane where they would ostensibly be available to participate in redox reactions.[18] Flavins are redox active, such that under reducing potential FMN (fluorescent) undergoes a $2H^+/2e^-$ transfer to $FMNH_2$ (nonfluorescent). Scheme 1 shows the structure of the isoalloxazine chromophore of FMN, which is fluorescent in the oxidized state, FMN, but much less so in the reduced state, $FMNH_2$. Thus, the fluorescence behavior of flavins

Research article
doi.org/10.1002/elsa.202100094
Chemistry Europe
European Chemical Societies Publishing

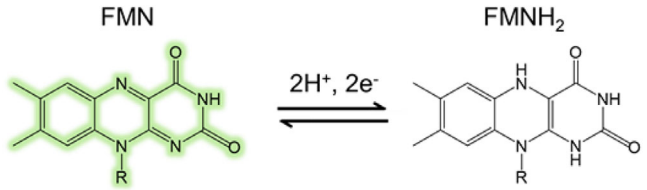

SCHEME 1 FMN reduction/oxidation

can be used to follow their redox state. Figure 2A shows the fluorescence image of a single *M. xanthus* bacterial cell on an ITO electrode, exhibiting inherent fluorescence, arising predominantly from flavins. Interestingly, the emission is spatially heterogeneous within the cell, with stronger fluorescence observed at the poles than at the center.

In order to follow redox activity of cell membrane-resident flavins, fluorescence intensity changes were tracked during potential sweeps in the range 0.6 V > E_{appl} > −0.6 V versus Ag/AgCl in 0.1 M PBS electrolyte. The cyclic voltammogram, Figure 2B, shows a typical non-Faradaic response in the +0.6 to −0.2 V range, with the current increase beyond −0.2 V being attributed to the onset of oxygen reduction. As shown in Figure 2C, fluorescence intensity was also monitored from a single bacterial cell as a function of time/potential and compared against the applied potential waveform. We plot these data as a normalized intensity contrast, $I_{norm} = [I - I_{min}]/[I_{max} - I_{min}]$ in order to draw attention to the potential-dependent intensity modulation. The corresponding raw intensity—potential trace data are shown in Supporting information Figure S1A. In all three potential sweep cycles, the fluorescence intensity peaks at the extreme reducing potential (−0.6 V) and drops at the oxidizing potential (+0.6 V). This observation is opposite to the expected potential-dependent fluorescence behavior of $FMN/FMNH_2$. In order to confirm this unexpected observation, potential step experiments were performed, in which the potential was stepped from 0.0 to 0.6 V and back in 0.1 V increments, holding for 10 s at each step. Supporting information Figure S1B shows that the fluorescence intensity decreases when the potential is stepped toward more positive/oxidizing potentials. Reversing the potential and stepping towards more negative/reducing potentials produces an increase in fluorescence intensity, consistent with the potential sweep experiments in Figure 2.

In order to understand the unexpected potential-dependent fluorescence behavior of *M. xanthus* on ITO, we performed cyclic potential sweep fluorescence measurements (0.0 V > E_{appl} > −1.0 V) of 10 μM FMN in 0.2 M KNO_3 in the presence of an ITO working electrode, as shown in Figure 3 (top panel). At low irradiance (3.5 W/cm^2, red trace in Figure 3), the normalized intensity contrast is constant at potentials more positive than −0.6 V, after which it decreases, consistent with the expected behavior based on the reduction of FMN to $FMNH_2$. During the reverse scan, I_{norm} increases in the range −1.0 to −0.6 V, then becomes essentially constant between −0.6 and 0.0 V, consistent with $FMNH_2$ being reoxidized to FMN. While this behavior is consistent with the theory and previous reports,[15,19] it is opposite to the behavior observed in *M. xanthus* on ITO.

Next, potential sweep experiments were performed on FMN at ITO under the same solution conditions but with increased laser irradiance. At an intermediate irradiance (32 W/cm^2, green trace in Figure 3), I_{norm} exhibits a complex behavior—increasing from −0.6 to −0.75 V, but then

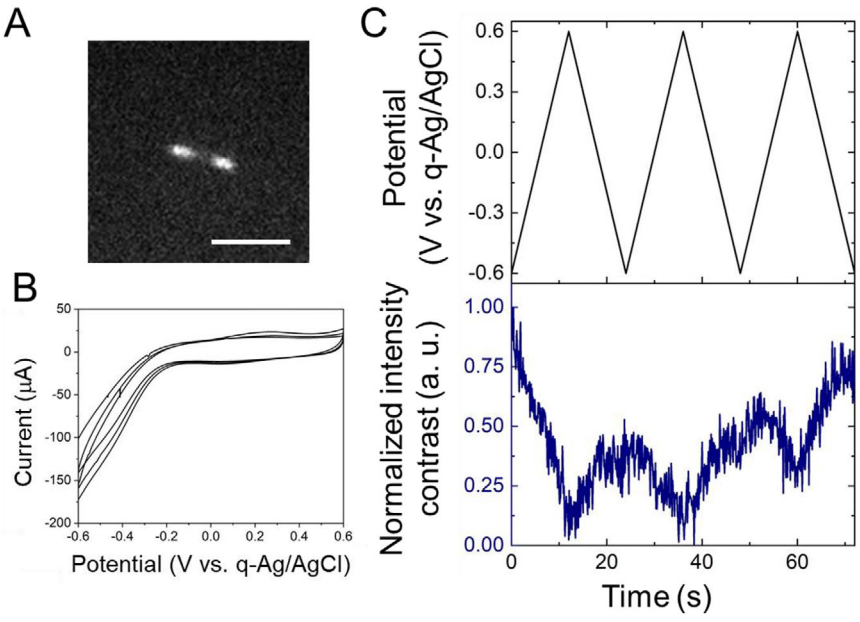

FIGURE 2 (A) Wide-field fluorescence image of single *M. xanthus* cell acquired with λ_{exc} = 458 nm (35 W/cm^2). Scale bar = 5 μm. (B) Cyclic voltammetry of M. *xanthus* on ITO electrode. (C) Applied potential waveform (top) and corresponding normalized fluorescence intensity contrast-time trace (bottom) for single M. *xanthus* on ITO electrode over three potential cycles 0.6 V > E_{appl} > −0.6 V versus Ag/AgCl scanned at 100 mV/s

Research article
doi.org/10.1002/elsa.202100094
Chemistry Europe
European Chemical Societies Publishing

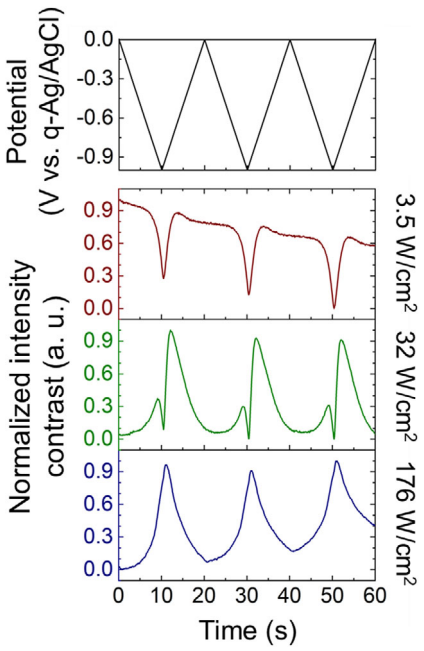

FIGURE 3 Applied potential waveform (top) and corresponding normalized fluorescence intensity contrast– time traces (bottom) in a cyclic sweep fluorescence experiment for 10 μM FMN in 0.2 M KNO_3. Response is recorded over three potential cycles 0.0 V > E_{appl} > −1.0 V versus Ag/AgCl scanned at 100 mV/s at three different laser power densities – 3.5 (red), 32 (green), and 176 W/cm^2 (blue). All fluorescence intensities normalized to the maximum value for that potential scan

rapidly decreasing as the scan continues to more negative potentials out to −1.0 V, followed by a sharp increase. The same biphasic behavior was observed in the two subsequent potential cycles. Further increasing the excitation irradiance (176 W/cm^2, blue trace in Figure 3), clearly shows anomalous behavior; I_{norm} increases during the negative-going portion of the scan to −1.0 V, peaking at the most negative potential, then decreases during the reverse scan from −1.0 V to 0.0 V. Clearly, the response of the FMN/ITO system changes phase going from low to high laser irradiance, with behavior at intermediate irradiance appearing to be an admixture of the low and high irradiance cases. The corresponding cyclic voltammogram of FMN, Supporting information Figure S2, shows that the electrochemical current response is independent of irradiance within experimental variation, specifically not showing the anomalous behavior observed in the cyclic sweep fluorescence experiments at medium and high irradiance values.

It is instructive to compare the behavior of the raw (unnormalized) emission intensity for varying excitation irradiance, as well its potential-dependent derivative, *dI/dV*. As shown in Supporting information Figure S3, it is apparent that the observed potential-dependent intensity variations are modest compared to the overall intensity—ranging from ca. 29% of the maximum intensity at 3.5 W/cm^2 to approximately 10% at 176 W/cm^2. The low irradiance data in Supporting information Figure S3A are consistent with the corresponding normalized low irradiance data in Figure 3, showing a negative *dI/dV* lobe at the most negative potentials. Furthermore, the intermediate irradiance data in Supporting information Figure S3B show the origin of the biphasic behavior is clearly the hysteresis between the negative- and positive-going branches of the *I*(*V*) curves. Finally, in contrast to the low irradiance behavior, the data in Supporting information Figure S3C exhibit a strong positive *dI/dV* lobe at the most negative potentials, as expected based on the normalized high irradiance data in Figure 3.

3.2 | Cyclic potential sweep fluorescence measurement of resorufin and Nile Blue

In order to further explore the unexpected cyclic sweep fluorescence behavior of the *M. xanthus*/ITO and FMN/ITO systems, similar measurements were performed using two different fluorophores that can be excited at different wavelengths—resorufin (λ_{ex} = 532 nm) and NB (λ_{ex} = 643 nm). The experiments were carried out using 10 μM of the fluorogenic probe in 0.2 M KNO_3. Consistent with the behavior of FMN, at low laser irradiance, I_{norm} decreases during the negative-going scan, reaching a minimum intensity at the negative end of the potential range, subsequently increasing during the reverse, that is, positive-going, scan for both resorufin and NB (Figure 4A and B, red traces, Supporting information Figures S4A and S5A). At high irradiance (Figure 4A and B, blue traces, Supporting information Figures S4C and S5C), both probes show an anomalous response, that is, maximum intensity at the negative end of the potential range, similar to that observed for FMN. In addition, at intermediate irradiance values both probes exhibit biphasic behavior (Figure 4A and B, green traces, Supporting information Figures S4B and S5B), near E_{appl} = −0.9/−0.8 V. The observation of similar irradiance dependence of the cyclic potential sweep fluorescence across all three fluorophores (Figures 3 and 4) suggests that the underlying mechanism responsible for the behavior is independent of excitation wavelength and the fluorogenic probe. Also, similar to FMN, the corresponding cyclic voltammograms of resorufin and NB (Supporting information Figure S6) do not show significant variation with laser irradiance.

To obtain more perspective on the behavior at intermediate and high irradiances, the cyclic potential sweep fluorescence measurements were repeated with different concentrations of NB (100, 500, and 1000 μM) at the three

Research article
doi.org/10.1002/elsa.202100094
Chemistry Europe
European Chemical Societies Publishing

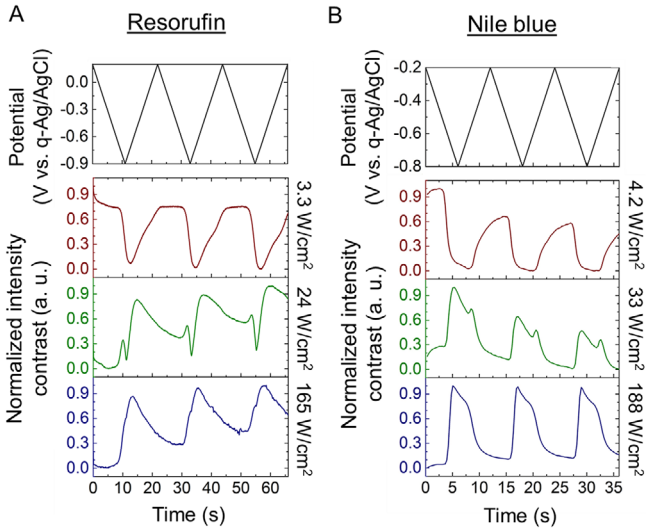

FIGURE 4 Applied potential waveform (top) and corresponding normalized fluorescence intensity contrast— time traces (bottom) of (A) 10 μM resorufin in 0.2 M KNO_3 and (B) 10 μM Nile Blue in 0.2 M KNO_3 over three potential cycles scanned at 100 mV/s at three different laser power densities as indicated

laser irradiance values used in Figure 4B. The results in Figure 5 show an interesting relationship between redox probe concentration and irradiance. First, at low irradiance (4.2 W/cm^2), irrespective of concentration, the canonical response (I_{norm} minimized at the negative end of the potential scan and maximized at the positive end) is observed. Second, at intermediate irradiance, 33 W/cm^2, high concentration solutions (500 and 1000 μM) show the canonical response, but low concentrations (10 and 100 μM) show the more complicated biphasic response. Last, at 188 W/cm^2, all four concentrations show inverse fluorescence potential response, with the 1000 μM solutions exhibiting the beginnings of a biphasic response. Taken together, these results clearly show that the fluorescence response is determined by a combination of laser irradiance and probe concentration. The unnormalized $I(V)$ and dI/dV data corresponding to conditions in Figure 5 are shown in Supporting information Figure S7.

3.3 | Photoluminescence of ITO

Given that the anomalous fluorescence response is independent of excitation wavelength and electrofluorogenic probe, the role of the ITO electrode was explored using cyclic potential sweep fluorescence measurements in electrolyte alone, that is, without electrofluorogenic probes. Employing PBS buffer and scanning over the range +0.6 V > E_{appl} > −0.6 V (Figure 6, red trace, and Supporting information Figure S8A) reveals that I_{norm} increases during the negative scan (+0.6 V to −0.6 V) reaching maximum intensity at the most negative potential followed by a decrease on the reverse scan (−0.6 V to +0.6 V). To address the possibility of low-level fluorescent contaminants in the PBS, 0.1 M phosphate buffer was freshly prepared and subsequently UV irradiated for 7 days in order to photobleach any fluorescent contaminants, but the response (Figure 6, green trace, and Supporting information Figure S8B) was unchanged. Last, the fluorescence

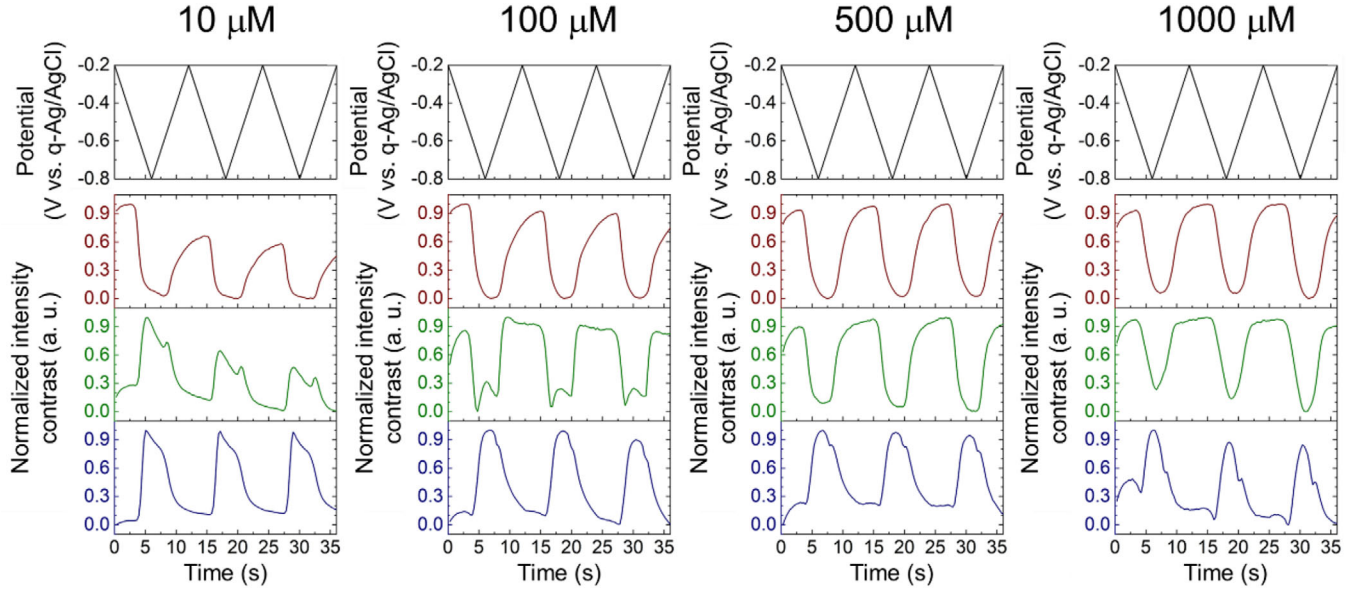

FIGURE 5 Applied potential waveform (top) and corresponding normalized fluorescence intensity contrast—time traces (bottom) for cyclic potential sweep fluorescence experiments executed on different concentration of Nile Blue in 0.2 M KNO_3. Data are presented over three potential cycles scanned at 100 mV/s at three different laser irradiance values: 4.2 W/cm^2 (red); 33 W/cm^2 (green); and 188 W/cm^2 (blue)

Research article
doi.org/10.1002/elsa.202100094
Chemistry Europe
European Chemical Societies Publishing

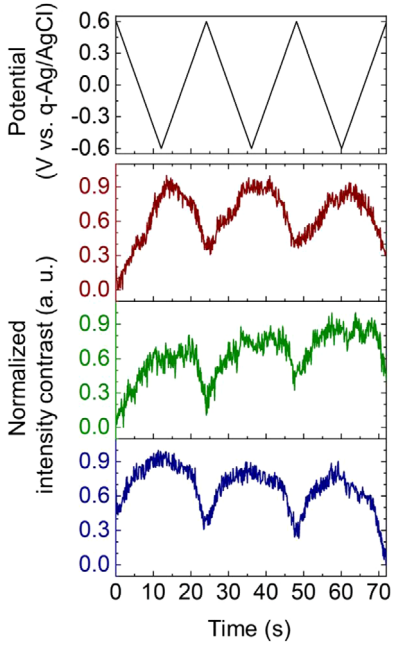

FIGURE 6 Applied potential waveform (top) and corresponding normalized luminescence intensity contras—ttime traces (bottom) of 0.1 M PBS (red), 0.1 M UV-photobleached phosphate buffer (green), and 0.2 M KNO_3 (blue) over three potential cycles scanned at 100 mV/s. λ_{exc} = 458 nm (35 W/cm^2)

behavior was also obtained for ITO in photobleached 0.2 M KNO_3 (Figure 6, blue trace, and Supporting information Figure S8C), and a similar behavior was observed. These experiments show that the potential-dependent fluorescence behavior is independent of the background electrolyte, leaving only ITO itself as the source of the potential-dependent I_{norm} behavior. It is also important to note that the cyclic voltammograms (Supporting information Figure S9) obtained in the absence of fluorophore show a typical capacitive response, confirming that ITO is not damaged by the laser radiation. Moreover, the scanning electron microscope images of ITO taken before and after the experiment (Supporting information Figure S10) show no apparent change in the morphology, confirming that the ITO is not affected by the reducing potentials.

The potential-dependent change in the ITO photoluminescence is clear, but the relative change in the signal is ≤4% over all three electrolytes. Even at high irradiance and scanning to the most negative potential, −1.0 V (Supporting information Figure S11), the fractional change for ITO photoluminescence is less than the fractional change observed for any of the fluorogenic probes (FMN ~10 %, resorufin ~8.6 %, and NB ~38 %). Thus, it is clear that, while it may play a minor role, the potential-dependence of ITO photoluminescence is not solely responsible for the anomalous potential-dependent emission behavior observed with the fluorogenic probes. However, we note that the luminescence observed from M. *xanthus* shows the same approximately 4 % change in the signal (Supporting information Figure S1A), so it is likely dominated by the potential-dependent ITO photoluminescence, rather than an anomalous response of the FMN.

3.4 | Redox probe spectroelectrochemistry—concentration dependence

While modulation of the ITO background can explain some of the anomalous spectroelectrochemical behavior, it is insufficient to describe all of our data, leading us to consider how the probe emission is affected by the combination of excitation irradiance, concentration, and potential. The potential-dependent emission intensity of redox probes is clearly dependent on both concentration and irradiance, with the inverted behavior at low concentration-high irradiance distinct from that at high concentration-low irradiance, as shown, for example, in Figure 5. We begin the concentration-dependent analysis by recognizing that all three dyes—FMN, resorufin, and NB—may adsorb at the ITO surface. Hypothesizing a Langmuir-like isotherm suggests that at low concentration there is a surface population, Γ_S, which is determined by a surface dissociation constant, K_D, and which, in turn, gives a characteristic ratio of surface-associated to free redox probe, Γ_S/Γ_F (Supporting information Figure S12A). As the solution concentration increases, the number of surface bound species increases as well, until saturation is reached, after which the surface population becomes independent of solution concentration (Supporting information Figure S12B). At this point, further increases in concentration simply increase the population of free redox probe, Γ_F, with no change in the surface-associated population, Γ_S (Supporting information Figure S12C). Turning to the potential dependence at high concentrations, we would expect it to be dominated by the behavior of free solution species, that is, responding to the canonical dependence of quantum efficiency on the oxidation state of the dye—namely, high emission intensity under oxidizing conditions and vice versa.

3.5 | Redox probe spectroelectrochemistry—irradiance dependence

Consistent with the adsorption isotherm hypothesis introduced above, at low solution concentration, some fraction of the dye population becomes surface-associated, and it is reasonable to assert that the observed behavior

Research article
doi.org/10.1002/elsa.202100094
Chemistry Europe
European Chemical Societies Publishing

is a combination of the intrinsic luminescence of ITO, as illustrated in Figure 6, and the interaction of the charge carriers in ITO with the surface-associated dye molecules. Understanding the potential-dependence of the intrinsic ITO emission begins with the absorption spectrum in Supporting information Figure S13, which shows strong absorption at $\lambda < 400$ nm due to the bandgap transition,[20] and a broad absorption feature in the 500-650 nm range that is assigned to a combination of donor-like and acceptor-like defect states.[21] The broad low-energy emission peak ranging from 500 to 650 nm, Supporting information Figure S13, overlaps the molecular emission of all three redox probes studied here and has been attributed to deep-level defects such as surface and oxygen defect (V_O) donor-like states and oxygen-indium vacancy pair (V_O-V_{In}) acceptors.[22] Furthermore, the unique conduction characteristics of ITO are associated with the presence of band tail states which arise in conjunction with the degenerate electronic character of the material.[23] When a reducing/negative potential is applied, the Fermi level is raised, which, because ITO is degenerate, increases the carrier concentration and, consequently the photoluminescence emission, consistent with the observations of intrinsic ITO luminescence in Figure 6.[24] Conversely, at oxidizing/positive potentials the carrier density decreases as does the photoluminescence intensity.

A complete explanation of the potential-dependent luminescence in the presence of electrofluorogenic redox probe must incorporate the interaction of the dynamic population of charge carriers in ITO with the surface-associated dye molecules, behavior which is most evident at low dye concentration and high irradiance. Not only does the normalized emission intensity contrast increase at negative potentials, but as shown in Supporting information Figure S3C, the absolute intensity does as well. Since this is opposite to the response one would expect based on the redox state of the dye, it suggests that the emission is dominated by surface-associated dye molecules, which exhibit a different potential/irradiance response than free dye. Irradiation of the ITO has the effect of increasing the available carriers, as does scanning the potential negative (raising the Fermi level). The simplest explanation would invoke charge transfer to the surface-associated dye molecule, thereby altering the electronic state of the molecule, similar to the chemical enhancement mechanism in surface-enhanced Raman scattering.[25] Thus, at high laser irradiance, emission from the adsorbed portion of the population is dominant and emission intensity increases. Supporting this hypothesis, Supporting information Figure S14 shows that the cathodic to anodic peak-to-peak separation for NB increases with scan rate at all concentrations and all laser irradiances, indicating electrochemical irreversibility. The formation of the surface-associated adsorbed redox probe is consistent with the observed electrochemical irreversibility.

4 | CONCLUSIONS

Under conditions of low irradiance and/or high redox probe concentration, cyclic potential sweep fluorescence measurements of three different electrofluorogenic probes—FMN, resorufin, and NB—at ITO working electrodes show reduced fluorescence intensities at more reducing potentials, consistent with the expectations based on the intrinsic luminescence efficiencies of oxidized and reduced forms of the dyes. However, at high irradiance an anomalous potential dependence is observed, especially at low concentration. At intermediate laser irradiances, a more complex behavior is observed in which the system exhibits a biphasic response at low concentrations before converting back to the canonical behavior at high concentration.

These observations suggest a model in which there are two distinct populations of dye molecules: (1) a freely diffusing population which dominates at higher concentration and gives rise to the canonical emission potential dependence, and (2) a surface-associated population in close electronic communication with the ITO working electrode. This latter population can respond to applied potential and irradiation through the formation of a charge transfer state whose electronic structure is distinct from free dye molecules. This combination of potential/irradiation-induced changes in the carrier dynamics of ITO, thus, gives rise to the noncanonical emission behavior in which dye luminescence intensity is a maximum at the most negative potentials.

These results should be useful in guiding others implementing low-concentration potential-dependent fluorescence experiments employing ITO as a working electrode. Additionally, the tentative identification of a charge transfer state as the emitting species on ITO at reducing potentials should open new avenues to explore the interaction between conducting metal oxide electrodes and dye molecules, which could be useful in engineering applications such as dye-sensitized solar cells.

CONFLICT OF INTEREST

The authors declare there are no conflict of interest.

ACKNOWLEDGMENTS

This work was supported by the Department of Energy Office of Science through Grant DE-SC0019312, by the National Institute of Health through Grant R01 AI113219-06, and by Notre Dame's Institute of Precision Health through a Harvest Grant.

DATA AVAILABILITY STATEMENT

The data that support the findings of this study are available from the corresponding author upon reasonable request.

REFERENCES

1. a) R. Hao, Y. Fan, M. D. Howard, J. C. Vaughan, B. Zhang, *Proc. Natl. Acad. Sci. USA* **2018**, *115*, 5878; b) V. Sundaresan, P. W. Bohn, *Chem. Sci.* **2020**, *11*, 10951; c) Y. Zhai, Z. Zhu, S. Zhou, C. Zhu, S. Dong, *Nanoscale* **2018**, *10*, 3089.
2. a) A. J. Cowan, L. J. Hardwick, *Annu. Rev. Anal. Chem.* **2019**, *12*, 323; b) N. E. Mendieta-Reyes, W. Cheuquepán, A. Rodes, R. Gómez, *ACS Catal.* **2020**, *10*, 103; c) I. Schmidt, A. Pieper, H. Wichmann, B. Bunk, K. Huber, J. Overmann, P. J. Walla, U. Schröder, *ChemElectroChem* **2017**, *4*, 2515.
3. a) K. A. Willets, A. J. Wilson, V. Sundaresan, P. B. Joshi, *Chem. Rev.* **2017**, *117*, 7538; b) S. Zaleski, A. J. Wilson, M. Mattei, X. Chen, G. Goubert, M. F. Cardinal, K. A. Willets, R. P. Van Duyne, *Acc. Chem. Res.* **2016**, *49*, 2023; c) A. J. Wilson, K. A. Willets, *Nano Lett.* **2014**, *14*, 939.
4. J. Lu, Y. Fan, M. D. Howard, J. C. Vaughan, B. Zhang, *J. Am. Chem. Soc.* **2017**, *139*, 2964.
5. J. B. Sambur, T.-Y. Chen, E. Choudhary, G. Chen, E. J. Nissen, E. M. Thomas, N. Zou, P. Chen, *Nature* **2016**, *530*, 77.
6. a) V. Brasiliense, A. N. Patel, A. Martinez-Marrades, J. Shi, Y. Chen, C. Combellas, G. Tessier, F. Kanoufi, *J. Am. Chem. Soc.* **2016**, *138*, 3478; b) F. T. Patrice, K. Qiu, Y. Ying, Y.T. Long, *Ann. Rev. Anal. Chem.* **2019**, *12*, 347; c) P. Saha, J. W. Hill, J. D. Walmsley, C. M. Hill, *Anal. Chem.* **2018**, *90*, 12832; d) V. Sundaresan, J. W. Monaghan, K. A. Willets, *ChemElectroChem* **2018**, *5*, 3052; e) J. D. Walmsley, J. W. Hill, P. Saha, C. M. Hill, *J. Anal. Test.* **2019**, *3*, 140; f) K. Wonner, C. Rurainsky, K. Tschulik, *Front. Chem.* **2020**, *7*, 912.
7. a) C. M. Hill, R. Bennett, C. Zhou, S. Street, J. Zheng, S. Pan, *J. Phys. Chem. C* **2015**, *119*, 6760; b) V. Sundaresan, J. W. Monaghan, K. A. Willets, *J. Phys. Chem. C* **2018**, *122*, 3138.
8. a) H. K. Ly, F. Harnisch, S. Hong, U. Schröder, P. Hildebrandt, D. Millo, *ChemSusChem* **2013**, *6*, 487; b) D. Millo, F. Harnisch, S. A. Patil, H. K. Ly, U. Schröder, P. Hildebrandt, *Angew. Chem. Int. Ed.* **2011**, *50*, 2625.
9. a) M. R. Bailey, A. M. Pentecost, A. Selimovic, R. S. Martin, Z. D. Schultz, *Anal. Chem.* **2015**, *87*, 4347; b) Y. Liu, H. Kim, R. R. Franklin, D. R. Bond, *ChemPhysChem* **2011**, *12*, 2235; c) J. C. P. d Souza, L. J. A. Macedo, A. Hassan, G. C. Sedenho, I. A. Modenez, F. N. Crespilho, *ChemElectroChem* **2021**, *8*, 431.
10. T. P. Lynk, C. S. Sit, C. L. Brosseau, *Anal. Chem.* **2018**, *90*, 12639.
11. Y. Yu, V. Sundaresan, S. Bandyopadhyay, Y. Zhang, M. A. Edwards, K. McKelvey, H. S. White, K. A. Willets, *ACS Nano* **2017**, *11*, 10529.
12. H. Kim, A. Piqué, J. S. Horwitz, H. Mattoussi, H. Murata, Z. H. Kafafi, D. B. Chrisey, *Appl. Phys. Lett.* **1999**, *74*, 3444.
13. a) Y. Fan, T. J. Anderson, B. Zhang, *Curr. Opin. Electrochem.* **2018**, *7*, 81; b) R. E. Palacios, F.-R. F. Fan, A. J. Bard, P. F. Barbara, *J. Am. Chem. Soc.* **2006**, *128*, 9028; c) A. J. Wilson, K. A. Willets, *Nano Lett.* **2014**, *14*, 939.
14. a) Z. Chen, W. Li, R. Li, Y. Zhang, G. Xu, H. Cheng, *Langmuir* **2013**, *29*, 13836; b) J. Du, X. Chen, C. Liu, J. Ni, G. Hou, Y. Zhao, X. Zhang, *Appl. Phys. A* **2014**, *117*, 815; c) K. Ellmer, *Nat. Photonics* **2012**, *6*, 809; d) S. Her, C. Chang, *J. Appl. Biomater. Funct. Mater.* **2017**, *15*, 170.
15. L. P. Zaino III, D. A. Grismer, D. Han, G. M. Crouch, P. W. Bohn, *Faraday Discuss.* **2015**, *184*, 101.
16. J. Hodgkin, D. Kaiser, *Mol. Gen. Genet.* **1979**, *171*, 177.
17. a) J. Hodgkin, D. Kaiser, *Proc. Natl. Acad. Sci. USA* **1977**, *74*, 2938; b) C. W. Harvey, C. S. Madukoma, S. Mahserejian, M. S. Alber, J. D. Shrout, *J. Bacteriol.* **2014**, *196*, 3853.
18. a) S. Cao, M. Wu, S. Xu, X. Yan, X. Mao, *J. Bacteriol.* **2015**, *197*, 1185; b) D. J. White, R. Merod, B. Thomasson, P. L. Hartzell, *Mol. Microbiol.* **2001**, *42*, 503.
19. D. Han, G. M. Crouch, K. Fu, L. P. Zaino III, P. W. Bohn, *Chem. Sci.* **2017**, *8*, 5345.
20. M. A. Blemker, S. L. Gibbs, E. K. Raulerson, D. J. Milliron, S. T. Roberts, *ACS Photon.* **2020**, *7*, 1188.
21. H. C. Weller, R. H. Mauch, G. H. Bauer, *Sol. Energy Mater. Sol. Cells* **1992**, *27*, 217.
22. M. Thirumoorthi, J. T. J. Prakash, *J. of Asian Ceram. Soc.* **2016**, *4*, 124.
23. C.H. Ho, C.H. Chan, L.C. Tien, Y.S. Huang, *J. Phys. Chem. C* **2011**, *115*, 25088.
24. Z. Sun, J. He, A. Kumbhar, J. Fang, *Langmuir* **2010**, *26*, 4246.
25. a) J. R. Lombardi, R. L. Birke, *J. Chem. Phys.* **2012**, *136*, 144704; b) R. L. Gieseking, M. A. Ratner, G. C. Schatz, *Faraday Discuss.* **2017**, *205*, 149; c) M. Yilmaz, E. Babur, M. Ozdemir, R. L. Gieseking, Y. Dede, U. Tamer, G. C. Schatz, A. Facchetti, H. Usta, G. Demirel, *Nat. Mater.* **2017**, *16*, 918.

SUPPORTING INFORMATION

Additional supporting information may be found online in the Supporting Information section at the end of the article.

How to cite this article: V. Sundaresan, A. R Cutri, J. Metro, C. S. Madukoma, J. D. Shrout, A. J. Hoffman, K. A. Willets, P. W. Bohn, *Electrochem. Sci. Adv.* **2021**, e2100094. https://doi.org/10.1002/elsa.202100094

Potential Dependent Spectroelectrochemistry of Electrofluorogenic Dyes on Indium-Tin Oxide

Vignesh Sundaresan[1#], Allison R Cutri[2#], Jarek Metro[2], Chinedu S. Madukoma[3,4], Joshua D. Shrout[3,4,5], Anthony J. Hoffman[6], Katherine A. Willets[7*], and Paul W. Bohn[1,2*]

[1]Department of Chemical and Biomolecular Engineering, University of Notre Dame, Notre Dame, IN 46556 USA

[2]Department of Chemistry and Biochemistry, University of Notre Dame, Notre Dame, IN 46556 USA

[3]Department of Civil and Environmental Engineering and Earth Sciences, University of Notre Dame, Notre Dame, IN 46556 USA

[4]Eck Institute for Global Health, University of Notre Dame, Notre Dame, IN, USA

[5]Department of Biological Sciences, University of Notre Dame, IN, USA

[6]Department of Electrical Engineering, University of Notre Dame, Notre Dame, IN 46556 USA

[7]Department of Chemistry, Temple University, Philadelphia, PA 19122 USA

[#]Equal contribution

[*]Authors to whom correspondence should be addressed, *kwillets@temple.edu*, *pbohn@nd.edu*

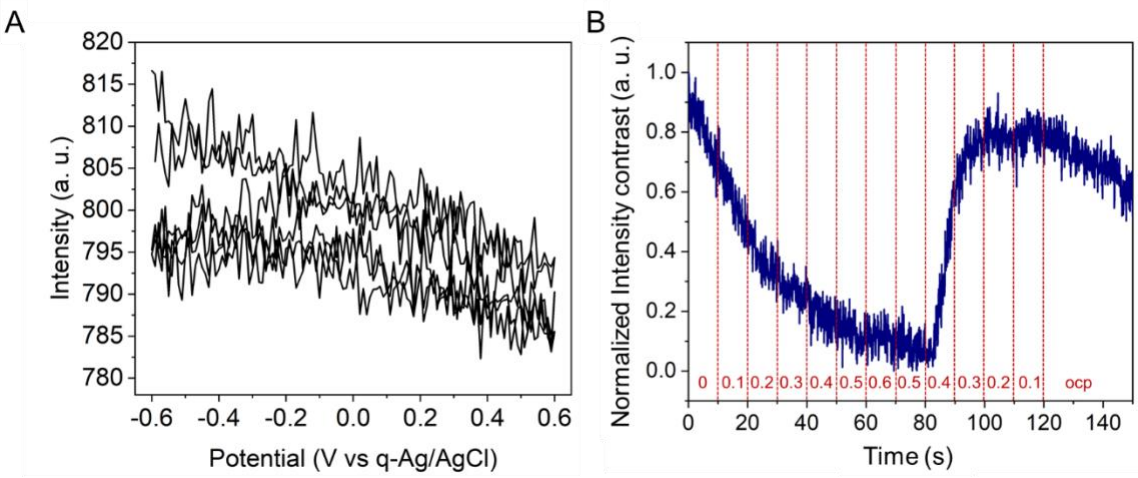

Figure S1. (A) Cyclic potential sweep fluorescence for the data shown in **Figure 2C**. (B) Potential step fluorescence time trace of a single *M. xanthus* cell. Potential was stepped from 0 to 0.6 V and back to 0 V with 0.1 V step and held for 10 s at each step. Applied potentials are labeled in red. The electrochemical cell was held at open-circuit potential (ocp) over the last 30 s.

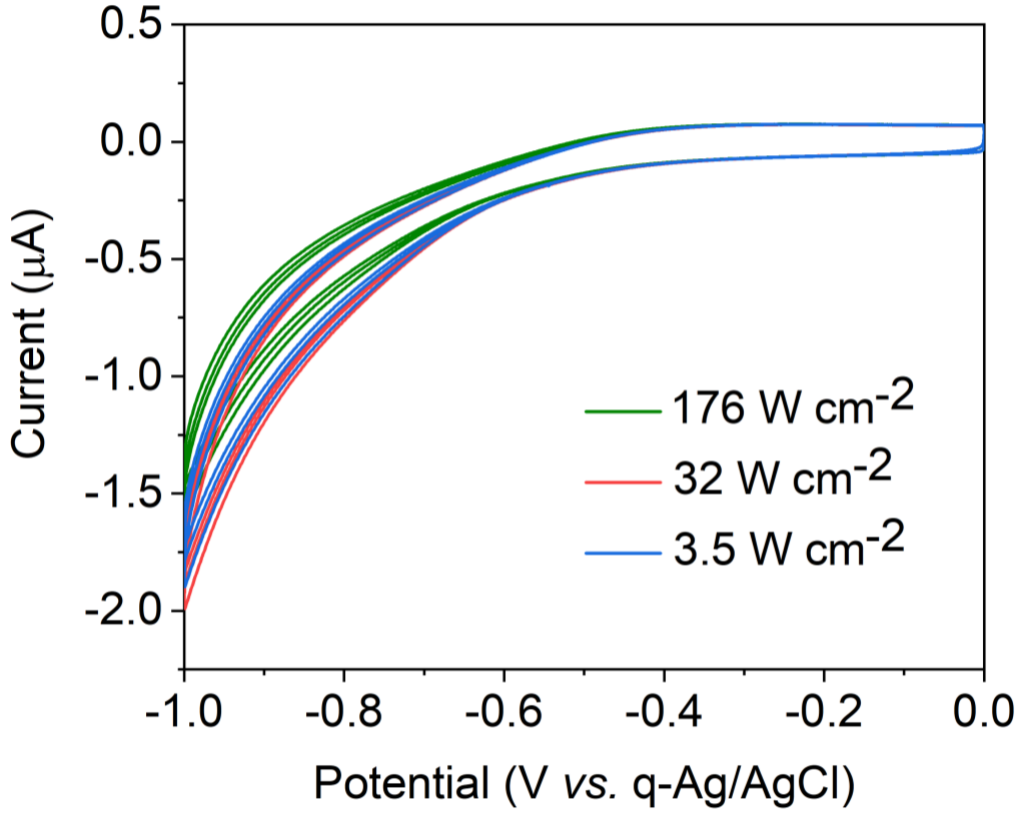

Figure S2. Cyclic voltammograms of 10 μM FMN in 0.2 M KNO_3 with an ITO working electrode in the presence of three different laser irradiance values.

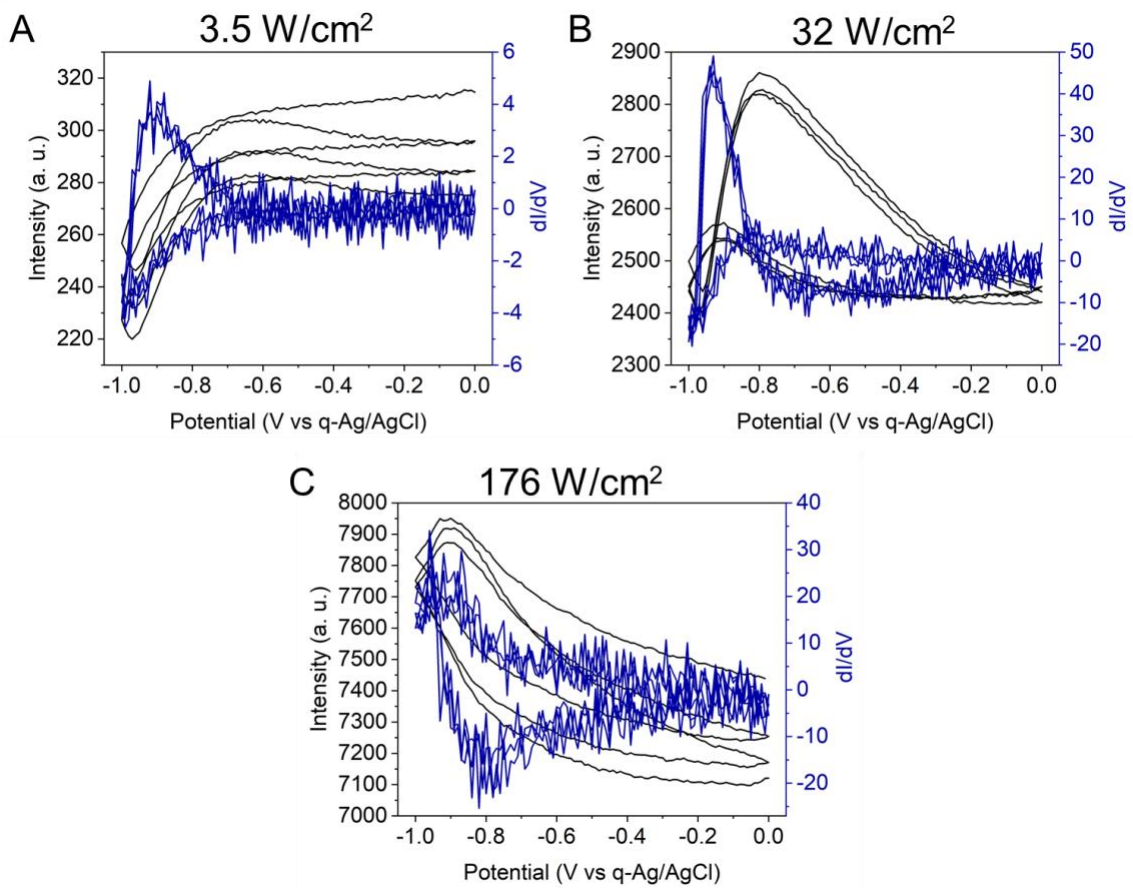

Figure S3. Cyclic potential sweep fluorescence (black) and fluorescence derivative, *dI/dV*, (blue) of 10 μM FMN in 0.2 M KNO_3 with an ITO working electrode for three laser irradiance values.

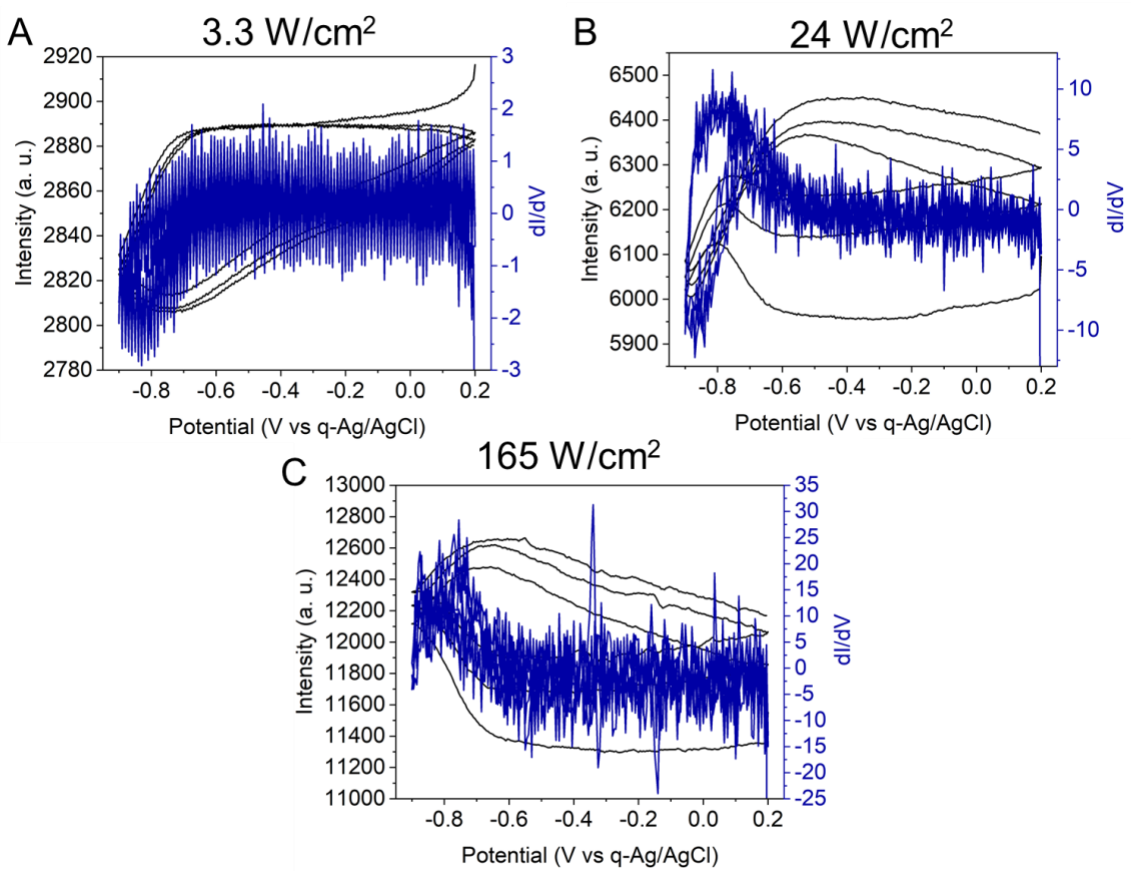

Figure S4. Cyclic potential sweep fluorescence (black) and fluorescence derivative, *dI/dV*, (blue) of 10 μM resorufin in 0.2 M KNO_3 with an ITO working electrode for three laser irradiance values.

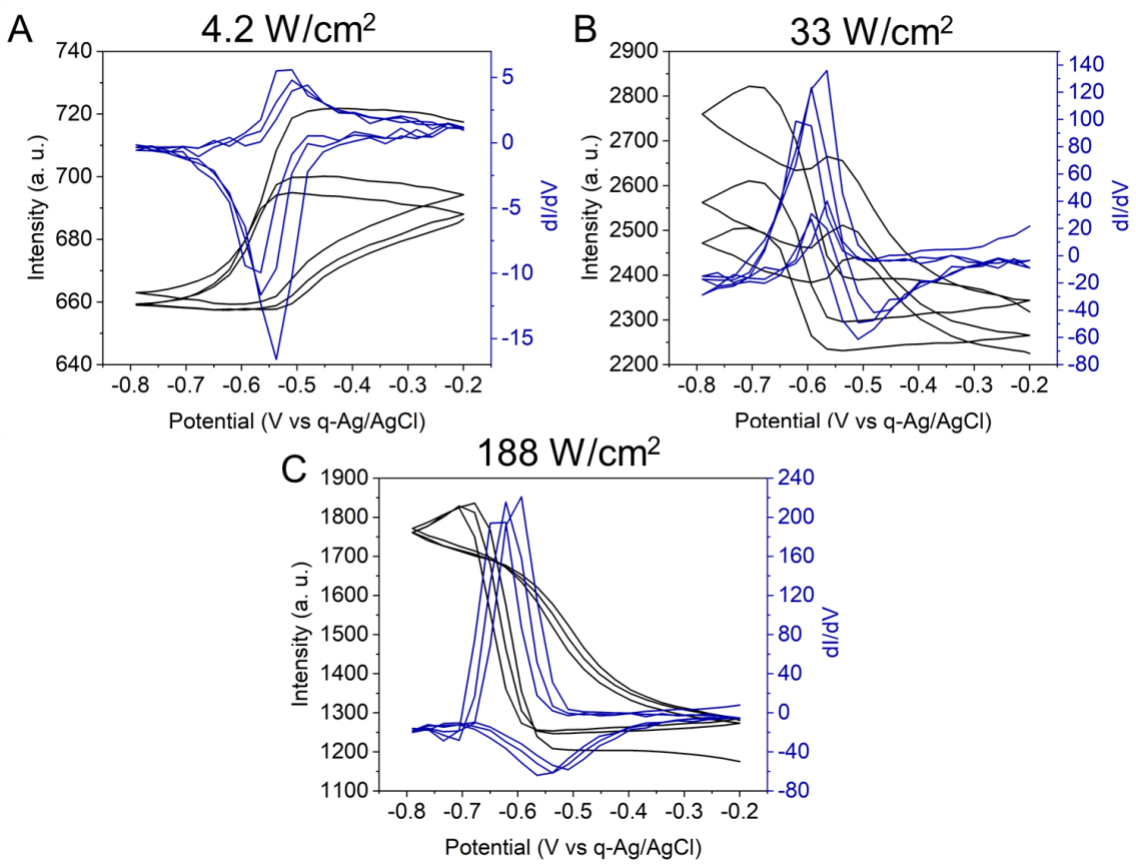

Figure S5. Cyclic potential sweep fluorescence (black) and fluorescence derivative, *dI/dV*, (blue) of 10 μM Nile Blue in 0.2 M KNO_3 with an ITO working electrode for three laser irradiance values. Note: the initial raw intensity at high laser irradiance (panel C) is smaller than the medium laser irradiance (panel B) because of the change in the electron multiplication (EM) gain in the EMCCD.

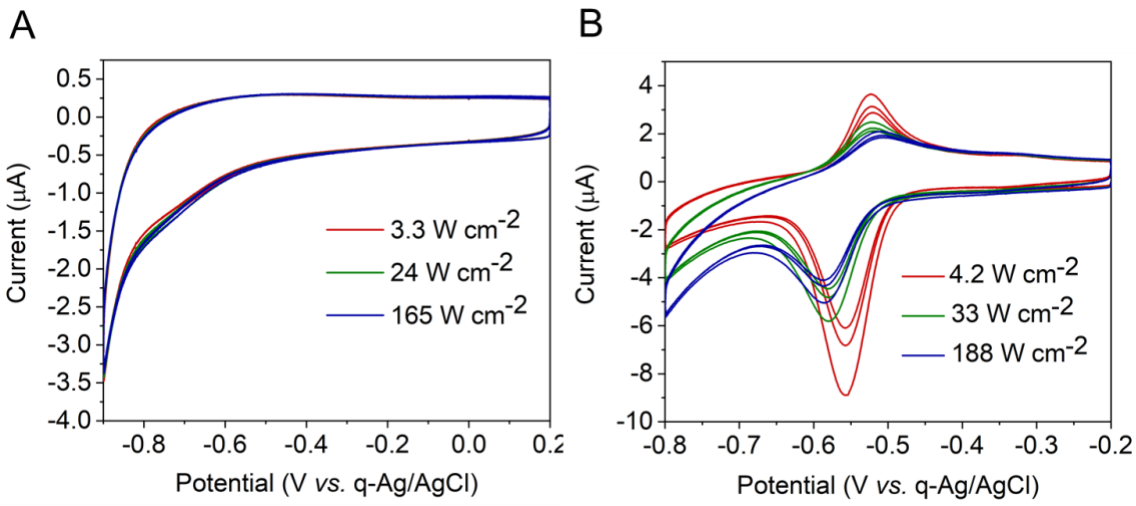

Figure S6. Cyclic voltammograms of (A) 10 μM resorufin in 0.2 M KNO_3, and (B) 10 μM Nile Blue in 0.2 M KNO_3 with an ITO working electrode in the presence of three different laser irradiance values.

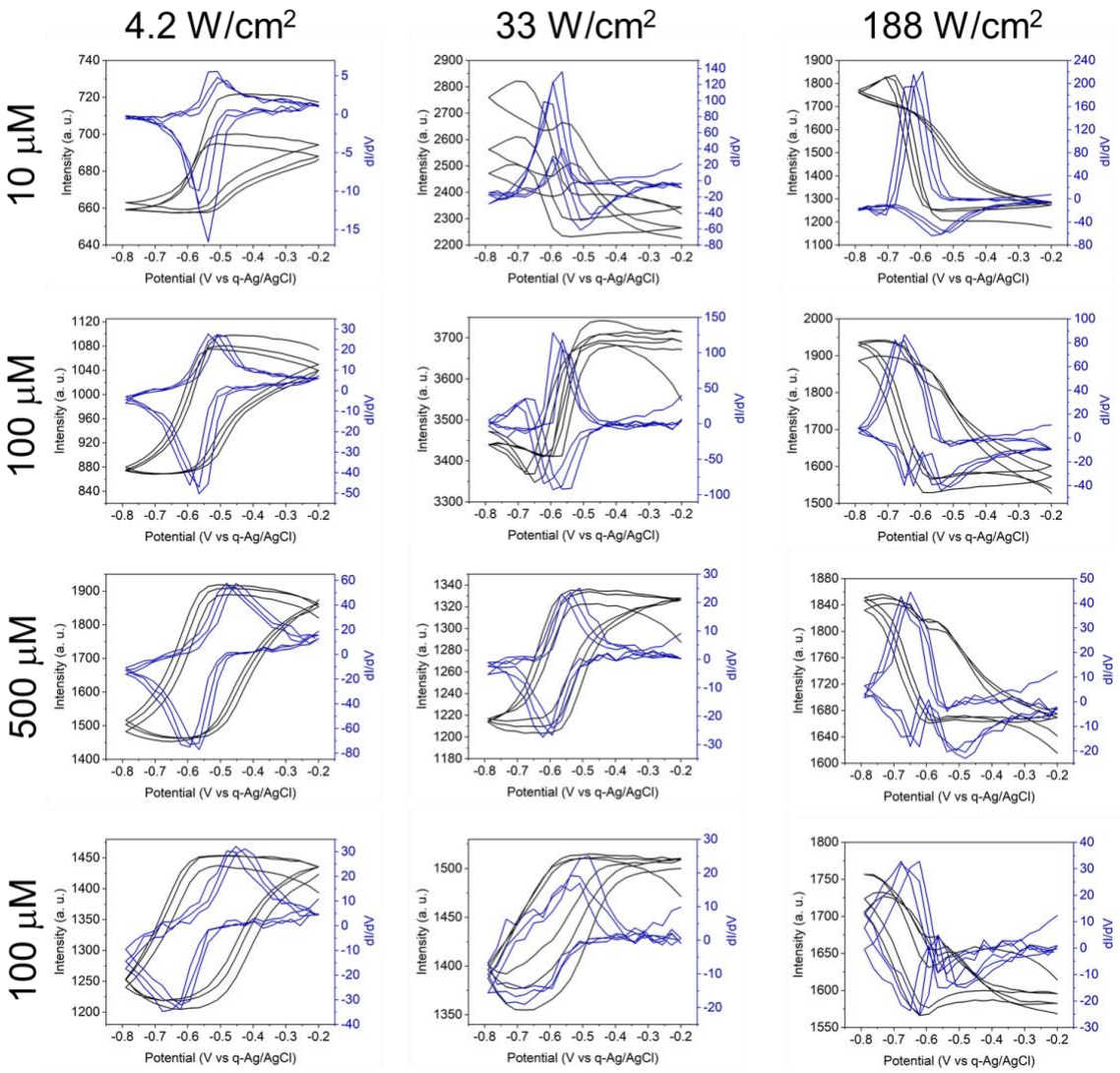

Figure S7. Cyclic potential sweep fluorescence (black) and fluorescence derivative, *dI/dV*, (blue) for different concentrations of Nile Blue in 0.2 M KNO_3 with an ITO working electrode for three laser irradiance values.

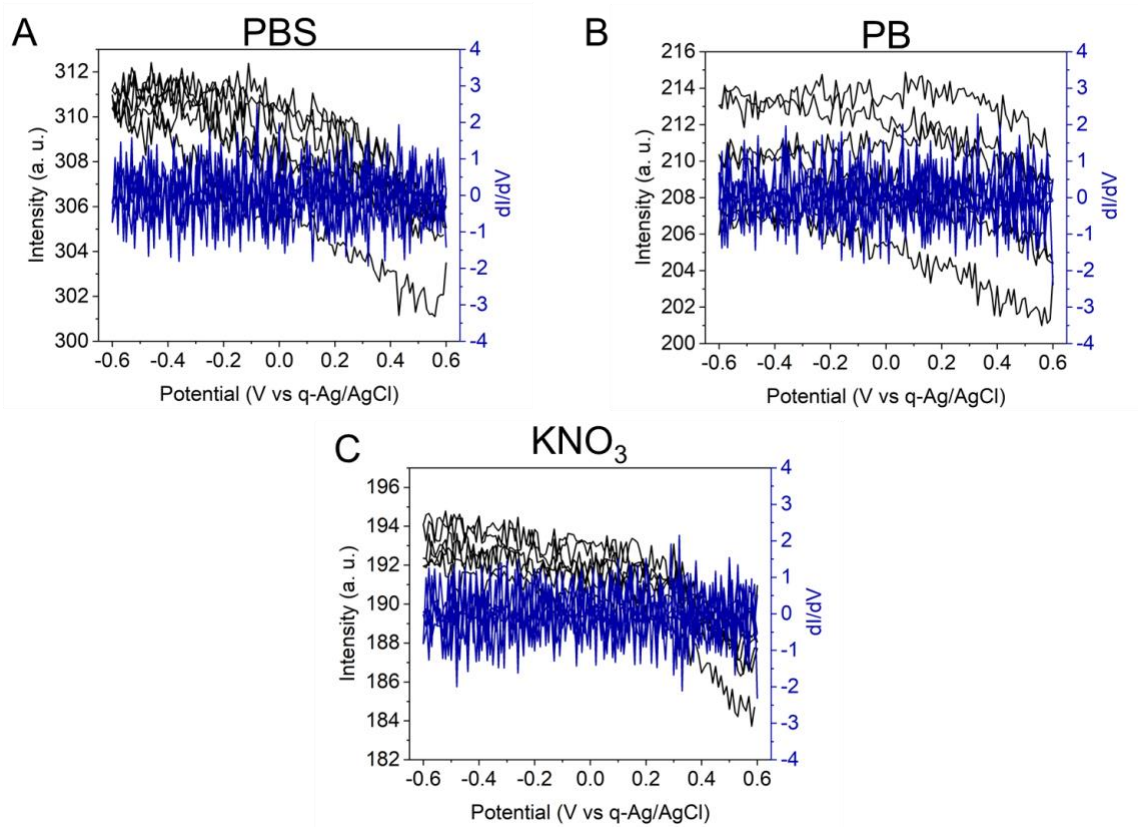

Figure S8. Cyclic potential sweep fluorescence (black) and fluorescence derivative, *dI/dV*, (blue) for ITO with (A) 0.1 M PBS, (B) 0.1 M UV-photobleached phosphate buffer, and (C) 0.2 M KNO_3 over three potential cycles scanned at 100 mV s^{-1}. λ_{ex} = 458 nm (35 W cm^{-2}).

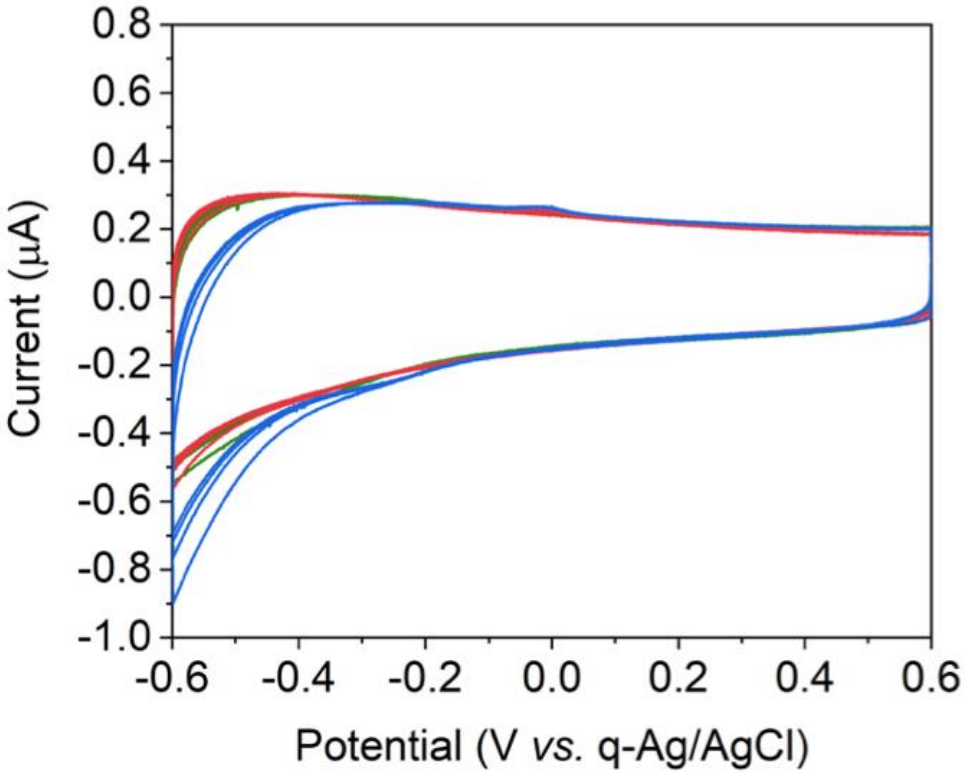

Figure S9. Cyclic voltammograms of an ITO electrode in 3 different electrolytes: 0.1 M PBS (green), 0.1 M photobleached PBS (red), and 0.2 M KNO_3.

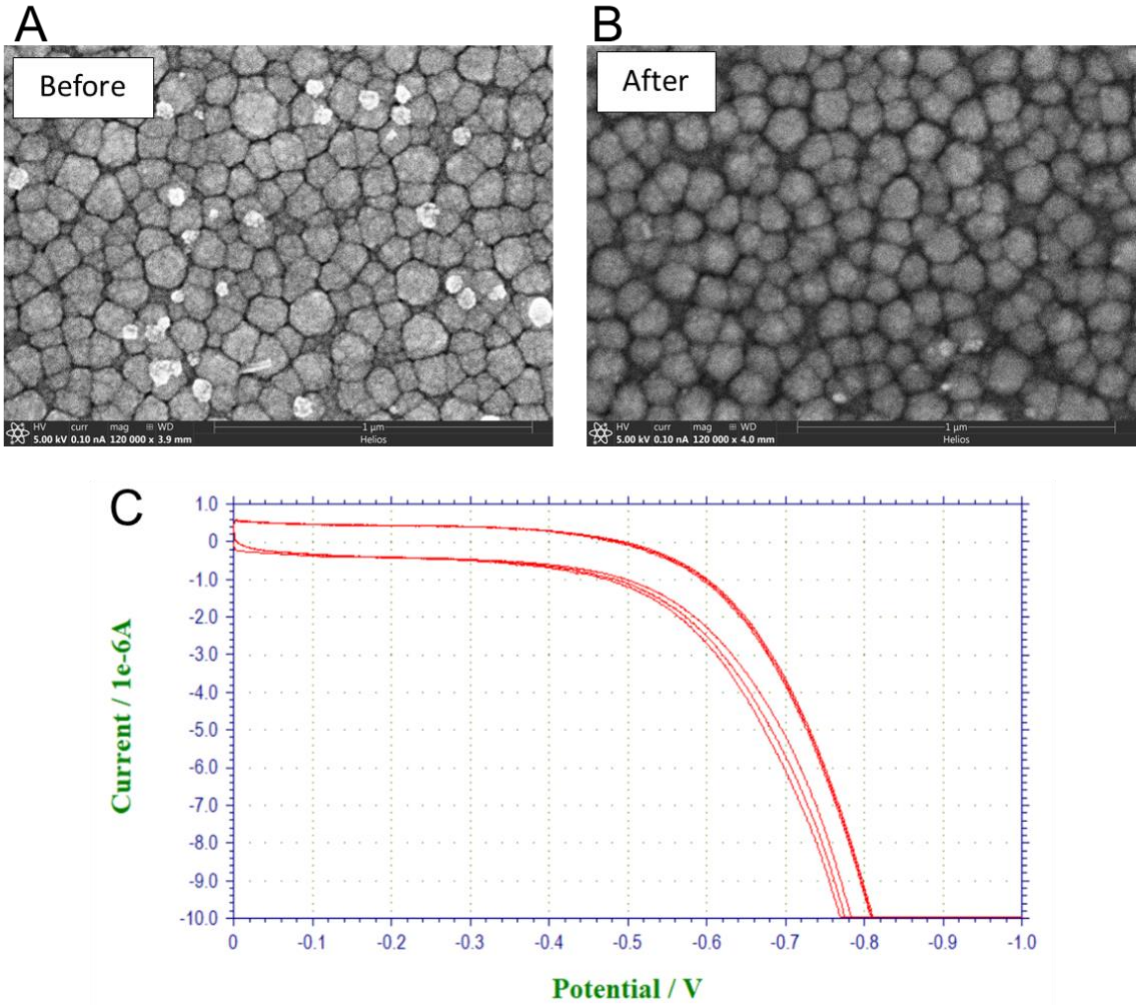

Figure S10. Scanning electron microscopy (SEM) images of ITO, (A) before and (B) after cyclic voltammetry in which the potential is scanned over the range 0 V ≥ E_{appl} ≥ -1 V in 0.2 M KNO_3 electrolyte over three cycles at 100 mV s^{-1}. (C) Corresponding cyclic voltammograms. The bright spots in panel A are tentatively assigned to impurities on the ITO surface, which are removed during potential cycling.

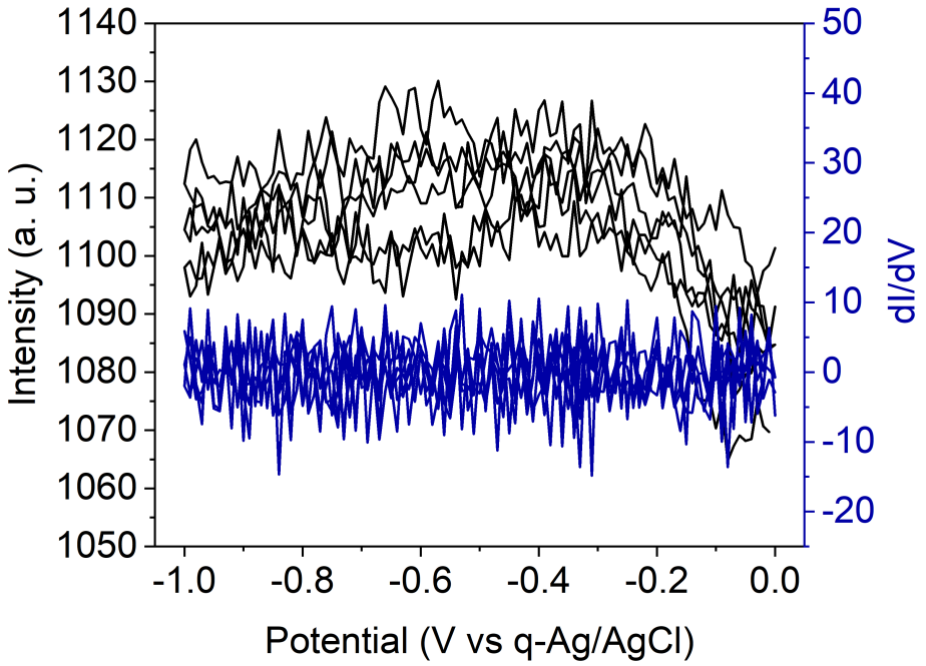

Figure S11. Cyclic potential sweep fluorescence (black) and fluorescence derivative, *dI/dV*, (blue) for ITO in 0.2 M KNO_3 over three potential cycles scanned at 100 mV s^{-1}. λ_{ex} = 458 nm (176 W cm^{-2}).

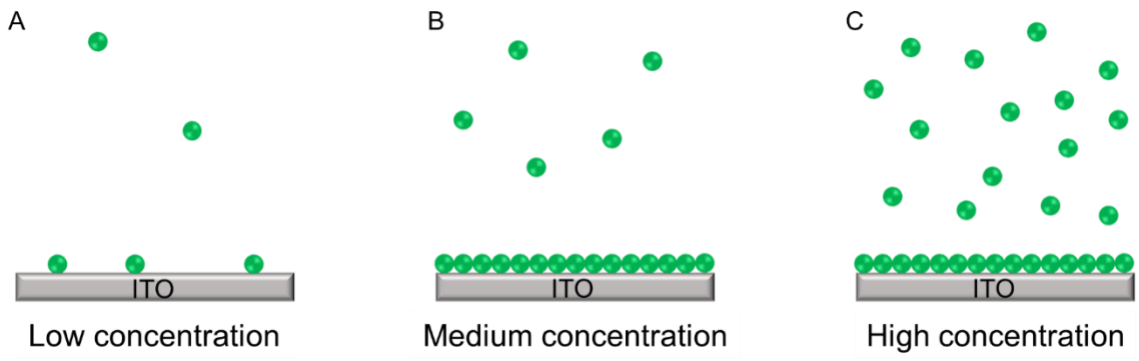

Figure S12. Schematic illustration of adsorption of dye molecules on ITO at three different concentrations.

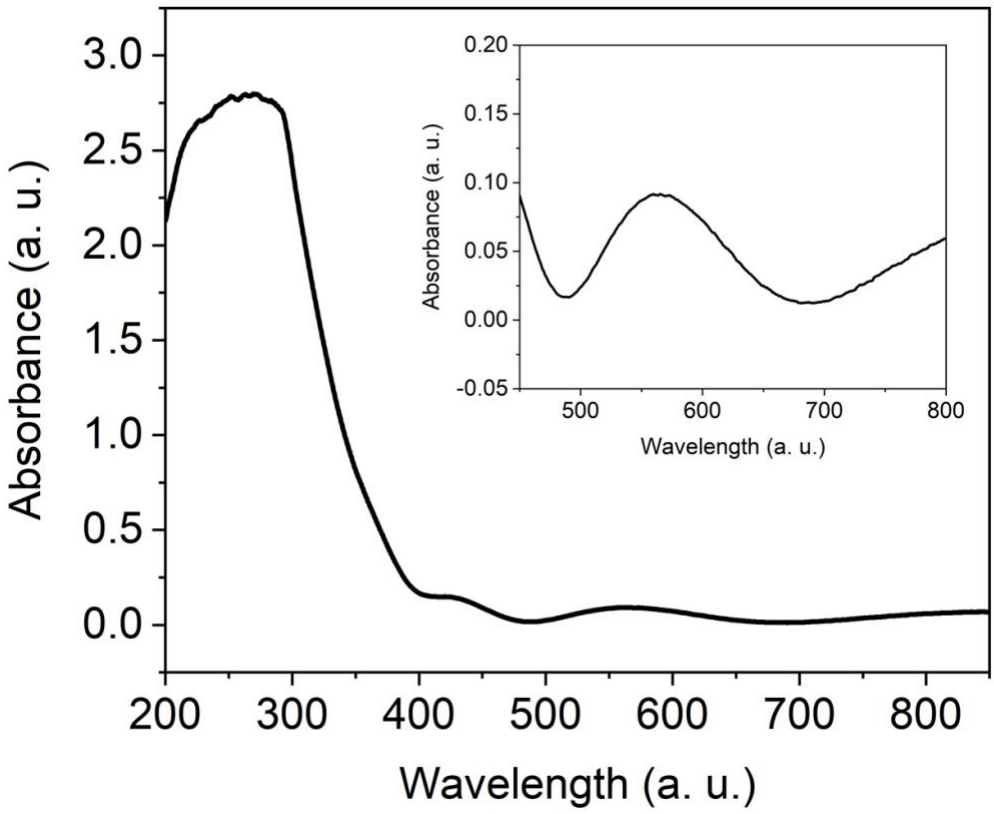

Figure S13. UV-Visible absorption spectrum of ITO coated glass. (*Inset*) Magnified view highlighting the absorption feature at 550-600 nm.

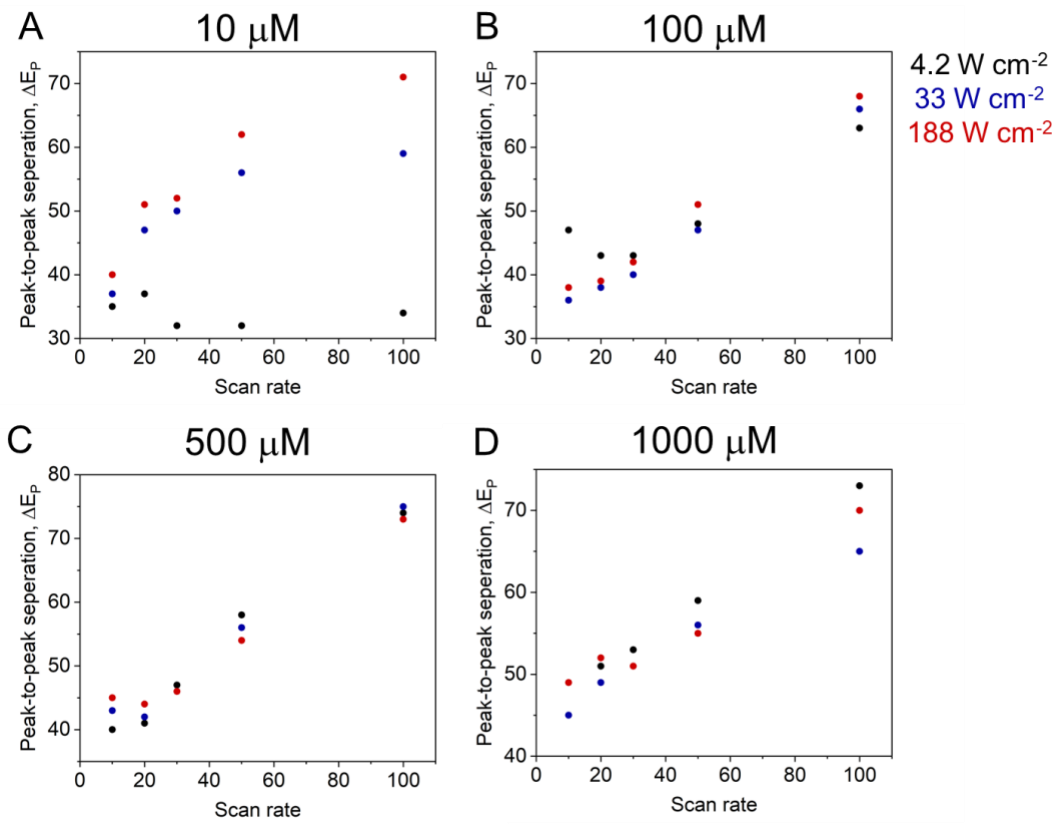

Figure S14. Cathodic to anodic peak-to-peak separation for different concentrations of Nile Blue in 0.2 M KNO_3 as a function of scan rate at different laser irradiance values (black 4.2 W cm^{-2}, blue 33 W cm^{-2}, red 188 W cm^{-2}).